# Influence of Metal Identity in Bipyridine-Based Metal-4N Complexes With Formate<sup>‡</sup>

Madison M. Foreman, Rebecca J. Hirsch, J. Mathias Weber\*

JILA and Department of Chemistry, University of Colorado Boulder, 440 UCB, Boulder, CO 80309-0440, USA

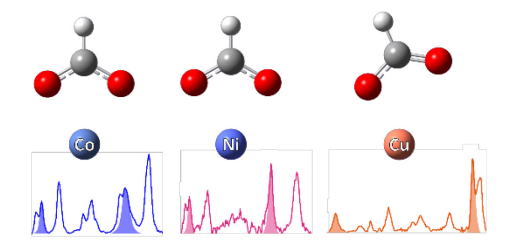
**AUTHOR INFORMATION** 

**Corresponding Author** 

\*weberjm@jila.colorado.edu, Tel.: +1-303-492-7841

ABSTRACT. We present the vibrational spectra of a series of dicationic, organometallic complexes consisting of a transition metal center (Co, Ni, or Cu) coordinated by 4,4'-di(*tert*-butyl)-2,2'-bipyridine (DTBbpy) ligands and a formate adduct. Spectral features are analyzed and assigned through comparison with density functional theory calculations, and structures are reported. Natural population analysis shows that the DTBBpy ligands serve as flexible charge reservoirs in each complex. Shifts in the vibrational signatures of the formate moiety reveal that the nature of the metal center plays a crucial role in the charge distribution and formate-metal binding motif in each complex, illustrating the impact of the metal center on the structural and electronic properties of these complexes.

#### **TOC GRAPHICS**



**KEYWORDS** Transition Metal Complexes; Cryogenic Ion Vibrational Spectroscopy.

#### Introduction

Transition metal complexes are ubiquitous in chemical applications, particularly in catalysis, due to their redox properties and compositional versatility.<sup>1-4</sup> Metal organic complexes are an attractive class of molecules for such applications, since their chemistry can first be roughly set by choice of the metal and the general framework of organic and/or inorganic ligands, and can then be fine-tuned by choosing derivatives of the ligands.<sup>5-7</sup> However, it is highly nontrivial to understand the mechanisms at play on a molecular level, or even characterize the main intermediates, since reactive mixtures under turnover conditions are very complex. Infrared spectroscopy in combination with quantum chemical calculations represents a widely used avenue for discerning molecular properties. In the condensed phase, however, particularly in reactive solutions, molecular-level details are often obscured due to solvent interaction, thermal broadening of spectral features, and speciation.

Many of the molecular catalysts and reaction intermediates under investigation by the catalysis community are ions, which are therefore accessible to mass spectrometry and its combination with laser spectroscopy. Electrospray ionization mass spectrometry in combination with laser spectroscopy offers an alternative approach, where ionic species of interest can be mass selected prior to applying spectroscopic probes, circumventing complications caused by speciation or the presence of counter ions and solvent molecules. In addition, cryogenic preparation of the target ions allows suppression of thermal broadening. Cryogenic ion vibrational spectroscopy (CIVS) has been used to great success by many groups, 8-21 and today represents a powerful part of the toolbox of cold chemistry.

In the present work, we put this method to use in the study of the structures and charge distributions of members of an important class of important organometallic complexes. In the complexes that are of interest here, a metal center is coordinated by four nitrogen atoms (M-4N complexes). Examples of these M-4N complexes used, e.g. as molecular catalysts, include porphyrins, phthalocyanines, and polypyridines, and the nature of the coordinating ligands heavily influences the redox properties of the compound.<sup>22-27</sup> These properties are crucial for their applications, e.g. in CO<sub>2</sub> reduction catalysis. In this particular application, several first- and second-row transition metals perform well, but there is particular interest in utilizing late first-row elements such as Co, Ni, and Cu due to their ubiquity and catalytic efficiency.<sup>28-31</sup> Like the nature of the ligand system, the identity of the metal center influences the functionality of the complex in several ways, as it impacts the coordination geometry and charge distribution of the complex, as well as the interaction with substrate and product molecules that are bound to the metal center during the catalytic cycle. It is therefore desirable to understand in detail how the nature of the metal center governs the structural and electronic properties of M-4N complexes.

In previous work,<sup>32</sup> we investigated the interaction of a cobalt center with 4,4'-di(*tert*-butyl)-2,2'-bipyridine (DTBbpy) ligands with and without the presence of a formate ion bound to the complex. In the present article, we revisit these complexes, providing both an improved analysis of these complexes regarding the possible spin states involved, and an additional investigation of the influence of the metal center on the geometry and charge distribution of complexes with the same ligands. To this end, we performed CIVS on complexes of the form  $[M \cdot (DTBbpy)_2 \cdot HCOO]^+$ , where M = Co, Ni, or Cu. We interpret our experimental results by comparison with predicted infrared spectra based on density functional theory (DFT) calculations.

#### Methods

## **Experimental**

Stock solutions of  $[M\cdot(DTBbpy)_2\cdot HCOO]^+$  (M = Co, Ni, Cu) were prepared by dissolving ca. 5–10 µmol of  $Co(NO_3)_2\cdot 6H_2O$ ,  $Ni(NO_3)_2\cdot 6H_2O$ , or  $Cu(NO_3)_2\cdot (H_2O)_3$  and ca. 10–20 µmol of DTBbpy (Sigma-Aldrich, 98%) in 5.75 mL of methanol (Macron,  $\geq$ 99.8%). Formate solution was prepared by titrating formic acid (Sigma-Aldrich,  $\geq$ 95%) with aqueous KOH (Fisher-Scientific) to a pH of 8–9 to ensure complete dissociation of the formic acid into formate anions. This solution was added to the stock solutions in an approximately 100:1 ratio of formate:  $[M\cdot(DTBbpy)_2\cdot HCOO]^+$  complexes. All chemicals were used as purchased, and all solutions were sprayed without further purification.

Only a brief overview of the cryogenic ion vibrational spectroscopy apparatus is provided here, as it has been described in detail previously.<sup>33</sup> Upon electrospray ionization of the solutions described above, gaseous complexes [M·(DTBbpy)2·HCO2]<sup>+</sup> were transferred through a series of octopole ion guides and ion optics into a cryogenically cooled 3D Paul trap held at ca. 30 K. In the trap, the ions were cooled by collisions with D<sub>2</sub> buffer gas and tagged with N<sub>2</sub> messenger molecules, which were present in the background gas coming from the electrospray source. The resulting [M·(DTBbpy)2·HCO2]<sup>+</sup>·N<sub>2</sub> clusters were then injected into a time-of-flight mass spectrometer, where they were mass-selected by an interleaving comb mass gate and then irradiated with the output of a pulsed tunable IR OPO/OPA system (LaserVision). Absorption of a photon and subsequent intramolecular vibrational relaxation led to the loss of the N<sub>2</sub> tag. The photofragment and parent ions were separated using a two-stage reflectron, and the [M·(DTBbpy)2·HCO2]<sup>+</sup> fragment intensity was detected by a double microchannel plate and monitored as a function of photon energy to acquire vibrational spectra. Ion signals were corrected

for photon fluence, and several spectra were taken on different days and averaged to ensure reproducibility and improve signal-to-noise ratio.

## **Computational**

Structures of  $[Co \cdot (DTBbpy)_2]^{2+}$  and of different isomers of  $[M \cdot (DTBbpy)_2 \cdot HCOO]^+$  (M = Co, Ni, Cu) were optimized in the framework of DFT, employing the B3LYP functional<sup>34</sup> and LANL2DZ basis sets<sup>35</sup> for all atoms in spin-unrestricted calculations (UB3LYP). We note that these calculations were costly, owing to the size of the molecules under study, and challenging, due to the electronic structure of the transition metals. Other approaches, including standard B3LYP, restricted open shell (RO)B3LYP, and ωB97XD<sup>36</sup>, as well as other basis sets (cc-pVDZ<sup>37</sup>, def2-SVP<sup>38</sup>, def2-TZVP<sup>38</sup>) produced a worse match to experimental spectra or failed to converge due to spin contamination, particularly in high-spin states, despite multiple attempts at adjusting the complex geometry. The least incomplete sets of results came from UB3LYP and ωB97XD functionals, both with 6-31G basis sets, and they are given in Supporting Information. Infrared spectra were calculated for converged structures with the same method and basis sets. The harmonic frequencies from these calculations were scaled by 0.975 to provide the best match to the experimental spectrum of [Co·(DTBbpy)2]2+, since the ligand vibrations proved to be least sensitive to the identity of the metal for all complexes. All calculations were performed using Gaussian 16.39

#### **Results and Discussion**

We begin by revisiting the spectra and structures of [Co·(DTBbpy)<sub>2</sub>]<sup>2+</sup> and its formate adduct, [Co·(DTBbpy)<sub>2</sub>·HCOO]<sup>+</sup>. In addition to the doublet states, which we studied in our previous work,<sup>32</sup> we have included quartet states in the present analysis, and the extension of our

computational analysis prompts us to change our assignment of the electronic structure of the metal and the structural assignment of the formate binding motif.

Figure 1 shows the comparison of the experimental spectrum of this complex and the calculated spectra for its high-spin and low-spin states. The vibrational modes of the DTBbpy ligands are well represented by both calculations. The only evidence for assigning a spin state for this complex is the fact that the quartet state is calculated to be higher in energy than the doublet state (see Table 1), suggesting that the doublet state is the most likely ground state of [Co·(DTBbpy)<sub>2</sub>]<sup>2+</sup>.

The assignment of the features is similar to that in our previous work.<sup>32</sup> At 1606 and 1615 cm<sup>-1</sup>, two partially resolved transitions belong to a combination of C–C stretching and in-ring-plane CH wagging motions in the bipyridine rings, which differ in their relative phases. The feature at 1536 cm<sup>-1</sup> contains several unresolved modes that are also largely localized on the bipyridine rings, and are characterized by antisymmetric C–N–C stretching motions, accompanied by CH wagging. The broad peak at 1479 cm<sup>-1</sup> contains several HCH bending modes that are largely localized on the *tert*-butyl part of the ligands. The sharp feature at 1413 cm<sup>-1</sup> is mainly due to bipyridine ring deformation modes that also involve CH<sub>3</sub> umbrella motions on the *tert*-butyl groups, with a low energy shoulder comprised of modes with CH wagging on the rings and tert-butyl methyl group umbrella motions. The feature at 1245 cm<sup>-1</sup> is mainly due to coupled C–C stretching modes throughout the complex.

The infrared spectrum of [Co·(DTBbpy)<sub>2</sub>]<sup>2+</sup> is compared with that of [Co·(DTBbpy)<sub>2</sub>·HCOO]<sup>+</sup> and the calculated spectra of the three lowest energy isomers in Figure 2. As described previously,<sup>32</sup> the modes of the DTBbpy ligands in [Co·(DTBbpy)<sub>2</sub>·HCOO]<sup>+</sup> exhibit small red shifts (< 20 cm<sup>-1</sup>) upon formate complex formation, while additional bands appear that can be identified as belonging to the formate ligand.

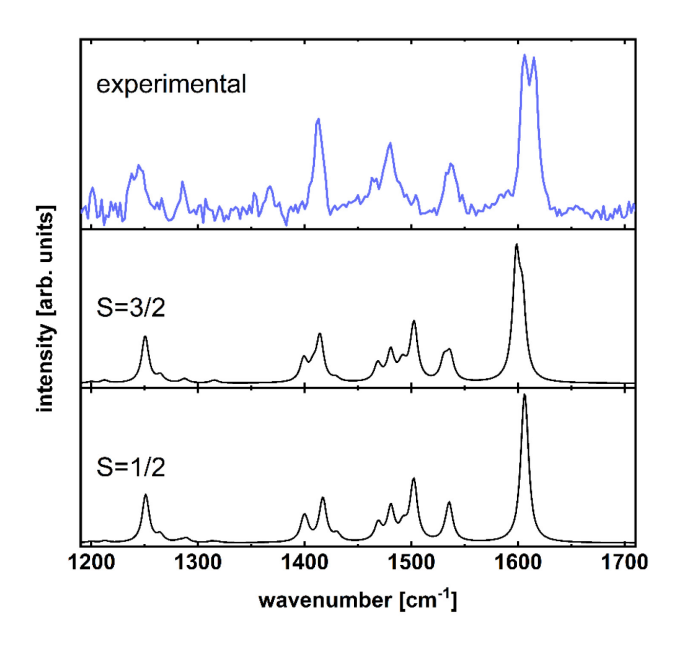
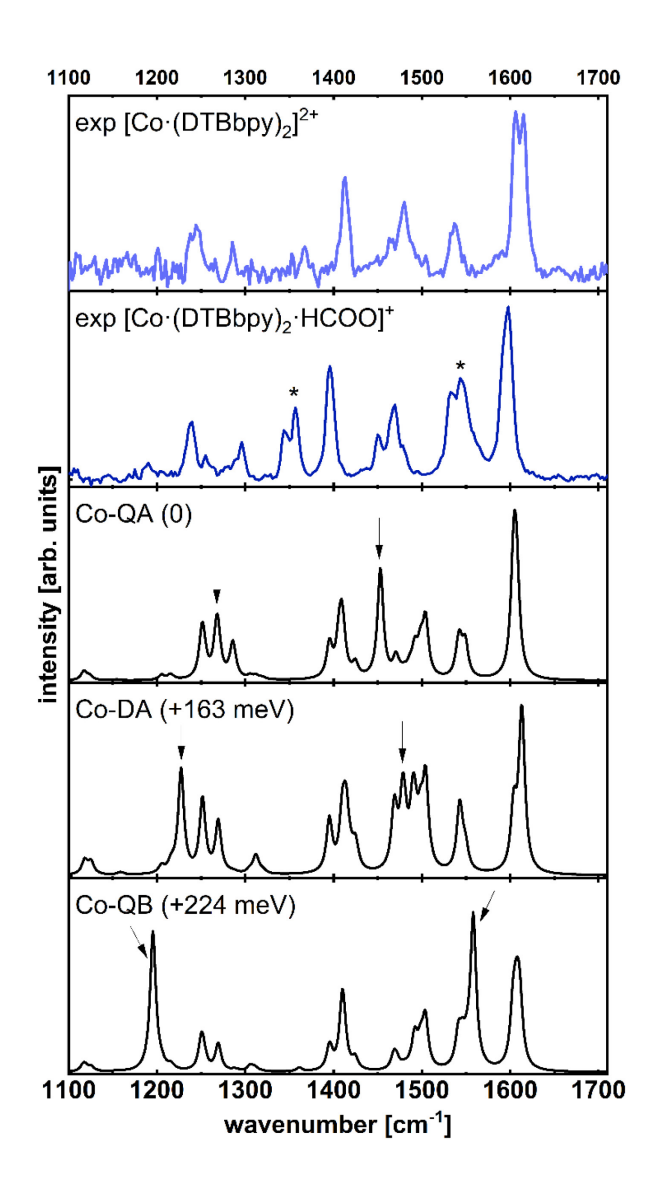


**Figure 1.** Comparison of the experimental spectrum (top trace, light blue) and calculated spectra (lower traces, black) of the doublet and quartet spin states of [Co·(DTBbpy)<sub>2</sub>]<sup>2+</sup>. Experimental data were taken from ref. 32. The calculated data are labeled with their spin states.

Table 1. Calculated energies and spin states of  $[Co\cdot(DTBbpy)_2]^{2+}$  and different isomers of  $[Co\cdot(DTBbpy)_2\cdot HCOO]^+$  complexes, as well as Co-O distances for the latter.

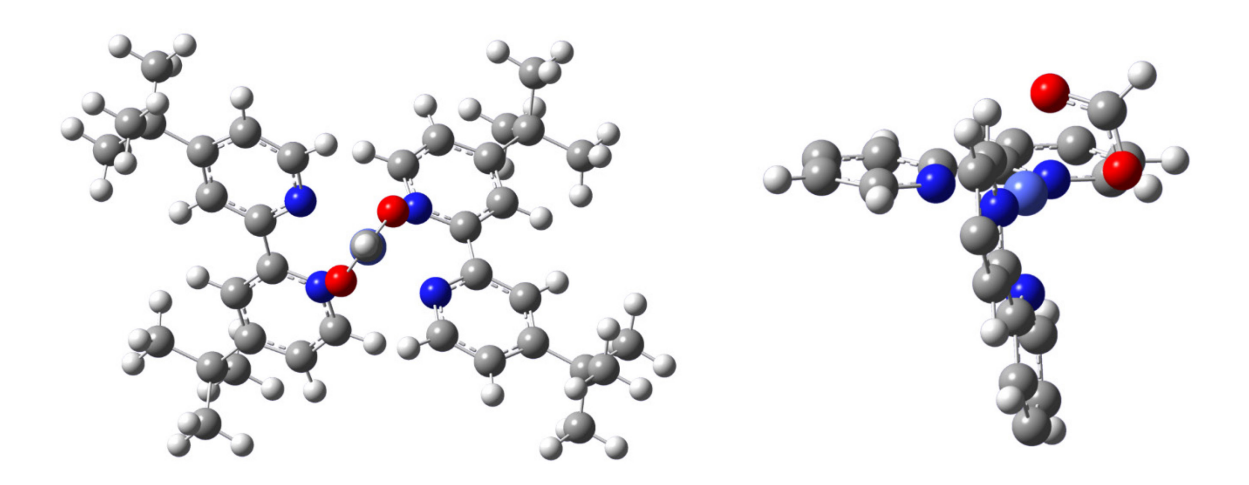
Complex	Spin	Relative Energy [meV]	Co-O [pm]
[Co·(DTBbpy) <sub>2</sub> ] <sup>2+</sup>	3/2	111	
	1/2	0	
[Co·(DTBbpy) <sub>2</sub> ·HCOO] <sup>+</sup>			
Isomer Co-QA	3/2	0	221
Isomer Co-QB		224	197, 336
Isomer Co-DA	1/2	163	200, 253
Isomer Co-DB		281	192, 335
Isomer Co-DC		380	192, 336

The lowest energy isomer of the formate complex (Co-QA) is in a quartet state (Table 1), with the formate ligand binding to the Co atom in a symmetric, bidentate fashion (Figure 3), while the other isomers bind asymmetrically to the metal, with varying degrees of asymmetry, and with varying orientations to the DTBbpy ligands (see Supporting Information for structures and calculated spectra of other isomers). The DTBbpy planes adopt a much more acute angle than in the bare catalyst complex, with the angle (measured as the N-metal-N angle indicated in Figure S1) changing from 152° in  $[\text{Co}\cdot(\text{DTBbpy})_2]^{2+}$  to 95°-100° in all isomers calculated for  $[\text{Co}\cdot(\text{DTBbpy})_2\cdot\text{HCOO}]^+$ . This geometry change is observed for all metals studied here with approximately the same calculated angles for  $[\text{M}\cdot(\text{DTBbpy})_2]^{2+}$  and  $[\text{M}\cdot(\text{DTBbpy})_2\cdot\text{HCOO}]^+$  (M = Co, Ni, Cu). All calculated structures adopt a distorted octahedral coordination of the metal atom.



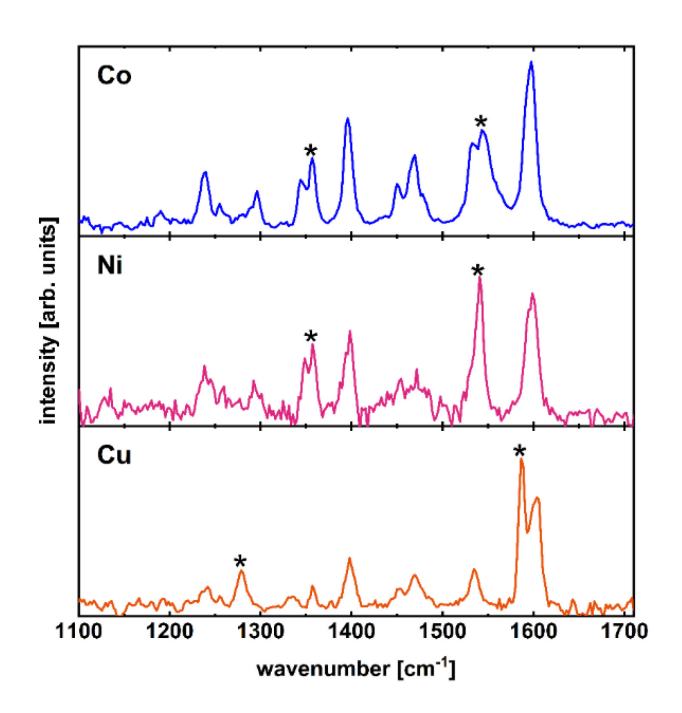
**Figure 2.** Comparison of the experimental spectra of  $[Co\cdot(DTBbpy)_2]^{2+}$  (top, light blue) and  $[Co\cdot(DTBbpy)_2\cdot HCOO]^+$  (second from top, dark blue) with calculated spectra for the three lowest energy isomers of  $[Co\cdot(DTBbpy)_2\cdot HCOO]^+$  (bottom traces, black, isomer labels and relative energies given as in Table 1). The signatures of the formate OCO stretching vibrations in the experimental spectrum are marked with asterisks, while their positions in the calculated spectra are marked with arrows, with  $v_s$  being the lower frequency feature. Experimental data were taken from ref. 32.

The average calculated frequencies of the formate OCO modes are significantly lower than for the experiment, despite the excellent agreement of the calculated spectra for the DTBbpy ligand features. This, too, is observed for all metals in the present work. Isomer Co-QA recovers the splitting between the symmetric (v<sub>s</sub>) and antisymmetric (v<sub>as</sub>) stretching modes quite well, while the other isomers do not (see Table S1). Isomers Co-QB, Co-DB, and Co-DC approximately recover the absolute position of  $v_{as}$  better, but they fail to predict  $v_{s}$  with any accuracy. Exploratory calculations regarding a possible influence of the N<sub>2</sub> tag on the frequency position either v<sub>s</sub> or v<sub>as</sub> found shifts to be less than 15 cm<sup>-1</sup>. We interpret the mismatch of the absolute frequencies for all calculations to be grounded in an underprediction of the CO bond strength in all cases. The method employed here recovers the OCO stretching frequencies of Ar-tagged formate somewhat better (experimental:  $v_s = 1314$  cm<sup>-1</sup> and  $v_{as} = 1622$  cm<sup>-1</sup>, <sup>40</sup> scaled harmonic frequencies: 1230 cm<sup>-1</sup> and 1567 cm<sup>-1</sup>), but also underestimates their absolute frequencies, while having better success with their splitting (337 cm<sup>-1</sup> calculated vs. 308 cm<sup>-1</sup> experimental). The reason for the unusually poor performance of the frequency calculations for the formate modes is unclear. These frequencies are sensitive to the partial charge in the carboxylate group, since the excess charge on the COO group resides in an overall antibonding orbital, weakening the CO bonds.<sup>41</sup> An overprediction of the amount of charge on the carboxylate group can therefore result in an underprediction of the CO bond strength. In contrast, the splitting between  $v_{as}$  and  $v_{s}$  reports more on the local symmetry of the CO bonds. Based on these arguments, we ascribe the mismatch between experimental and calculated formate frequencies to a misrepresentation of the charge distribution in the formate moiety. However, we judge that the bidentate formate-metal interaction in isomer Co-QA best describes the actual structure of the complex, and that the complex adopts a quartet ground state.

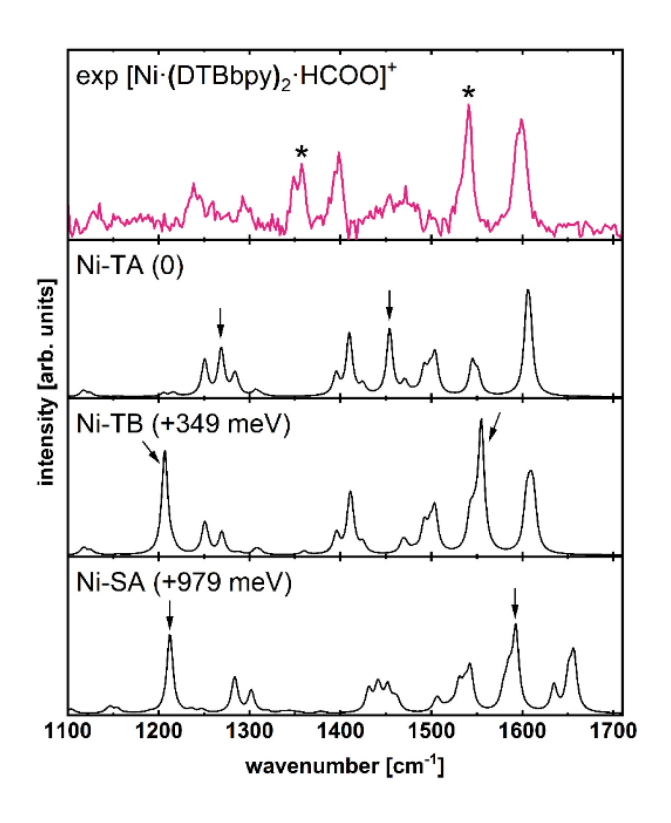


**Figure 3.** Lowest energy structure of  $[Co \cdot (DTBbpy)_2 \cdot HCOO]^+$  (isomer Co-QA). **Left:** Structure viewed along the CH bond axis of the formate ligand to highlight the orientation of the formate relative to the metal atom. **Right:** Structure viewed from the side to highlight formate orientation relative to DTBBpy ligands, whose methyl groups are omitted for clarity. Color scheme: H = White, C = Gray, N = Gra

Figure 4 shows a comparison of the experimental spectra of [M·(DTBbpy)<sub>2</sub>·HCOO]<sup>+</sup> (M = Co, Ni, Cu). The features belonging to the DTBbpy ligands are identical within the bandwidth of our light source, suggesting that the geometries of these ligands are similar for each complex The calculated structures reflect this similarity, with the lowest energy isomers for each metal having approximately the same N-Metal-N angles (ca. 100°). Given the similarity of the DTBbpy features in all the spectra, the positions of the formate OCO stretching modes were easily determined by identifying peaks that were different from the previously identified DTBbpy modes. The cobalt and nickel complexes have very similar formate OCO stretching modes, indicating that the formate should bind similarly to the metal in both cases.



**Figure 4.** Comparison of the spectra of  $[M \cdot (DTBbpy)_2 \cdot HCOO]^+$  (M = Co, Ni, Cu). Metal identity is given in each panel (Co = dark blue, Ni = pink, Cu = orange). The positions of  $v_s$  and  $v_{as}$  are identified in each case by asterisks.



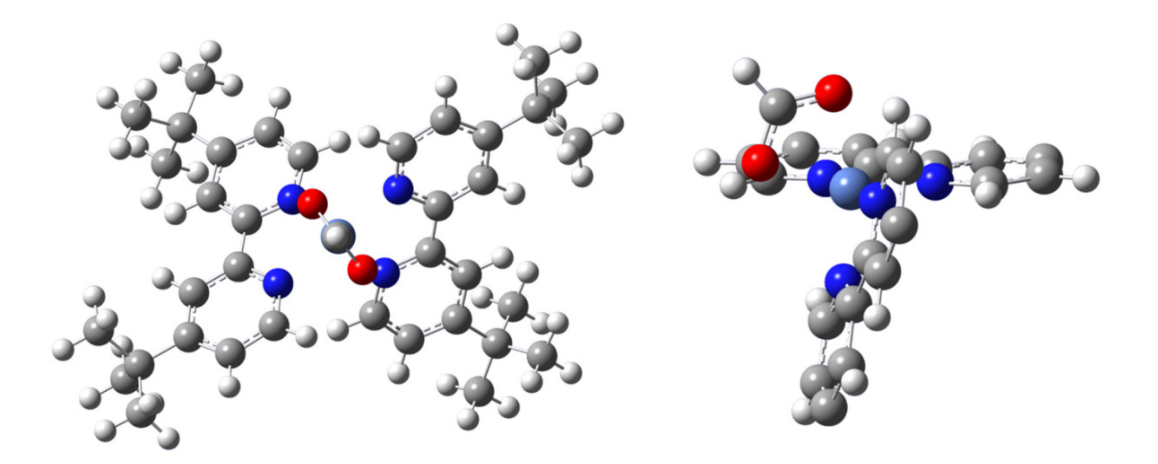
**Figure 5.** Comparison of the experimental spectrum of  $[Ni\cdot(DTBbpy)_2\cdot HCOO]^+$  (top trace, pink) with calculated spectra for selected isomers (lower traces, black, isomer labels and relative energies given as in Table 2). The signatures of the formate OCO stretching vibrations in the experimental spectrum are marked with asterisks, while their positions in the calculated spectra are marked with arrows, with  $v_s$  being the lower frequency feature.

Table 2. Calculated energies, spin states, and Ni-O distances for different isomers of [Ni·(DTBbpy)<sub>2</sub>·HCOO]<sup>+</sup> complexes.

Complex	Spin	Relative Energy [meV]	Ni-O [pm]
Isomer Ni-TA	1	0	217
Isomer Ni-TB		349	197, 334
Isomer Ni-TC		384	197, 340
Isomer Ni-SA	0	979	190, 302
Isomer Ni-SB		1027	189, 335
Isomer Ni-SC		1152	189, 325

The comparison between the experimental spectrum of [Ni·(DTBbpy)2·HCOO]<sup>+</sup> and the calculated spectra of three selected isomers is presented in Figure 5 (see Table 2 and Supporting Information for energies of additional isomers). The [Ni·(DTBbpy)2·HCOO]<sup>+</sup> complex can exist in triplet or singlet states. In analogy to the Co complexes, the energies of the high-spin states are lowest in energy, with singlet states of the formate complexes calculated to be significantly (ca. 1 eV) higher than those of the triplet states. Interestingly, the [Ni·(DTBbpy)2]<sup>2+</sup> catalyst without the formate is calculated to have a singlet ground state 355 meV lower than the corresponding triplet, indicating that formation of the formate complex switches the spin state of the metal.

In line with the similarity of their spectra, the structure of the lowest energy isomer (Ni-TA) is similar to Co-QA, as the formate binds in a symmetric, bidentate fashion to the Ni atom (see Supporting Information for structures and spectra of the calculated isomers). Identification of the spin state is very clear for the Ni complexes, since the calculated frequencies of the highest energy DTBbpy modes (C-C stretching and in-ring-plane CH wagging motions of the bpy rings) are predicted to be much higher in frequency than what would be compatible with the experimental spectrum. In light of the excellent recovery of the DTBbpy modes by the triplet structures, assignment of the spectrum to the triplet state is unambiguous, and in agreement with their relative energies. However, the description of the formate signatures by the calculated spectra suffers from the same inconsistencies as for the Co complex. The lowest energy isomer recovers the splitting between v<sub>s</sub> and v<sub>as</sub> nearly quantitatively, but the absolute energies are predicted to be too low (Table 2). The other calculated triplet structures recover v<sub>as</sub> well, but completely fail for v<sub>s</sub>. Following the same logic as for the Co complexes, we therefore ascribe the spectrum to the lowest energy isomer, Ni-TA (structure shown in Figure 6).



**Figure 6.** Lowest energy structure of  $[Ni\cdot(DTBbpy)_2\cdot HCOO]^+$  (isomer Ni-TA). **Left:** Structure viewed along the CH bond axis of the formate ligand to highlight the orientation of the formate relative to the metal atom. **Right:** Structure viewed from the side to highlight formate orientation relative to DTBBpy ligands, whose methyl groups are omitted for clarity. Color scheme: H = White, C = GRAY, N = WARDER AND COLOR AND COLOR

The ground state electron configuration of the copper complexes [Cu·(DTBbpy)2·HCOO]<sup>+</sup> can only adopt doublet spin states, removing one of the challenges in the description of the other two metals in this series. Similar to the other metals in this study, the spectrum of the lowest energy isomer, Cu-A, best captures the splitting of v<sub>s</sub> and v<sub>as</sub> of the formate ligand, but underpredicts the absolute frequencies (Figure 7). The corresponding structure is shown in Figure 8. Different from the Co and Ni complexes in this work, the formate ligand binds asymmetrically to the metal (see Supporting Information for structures of the other calculated isomers), but the structure can still be seen as bidentate.

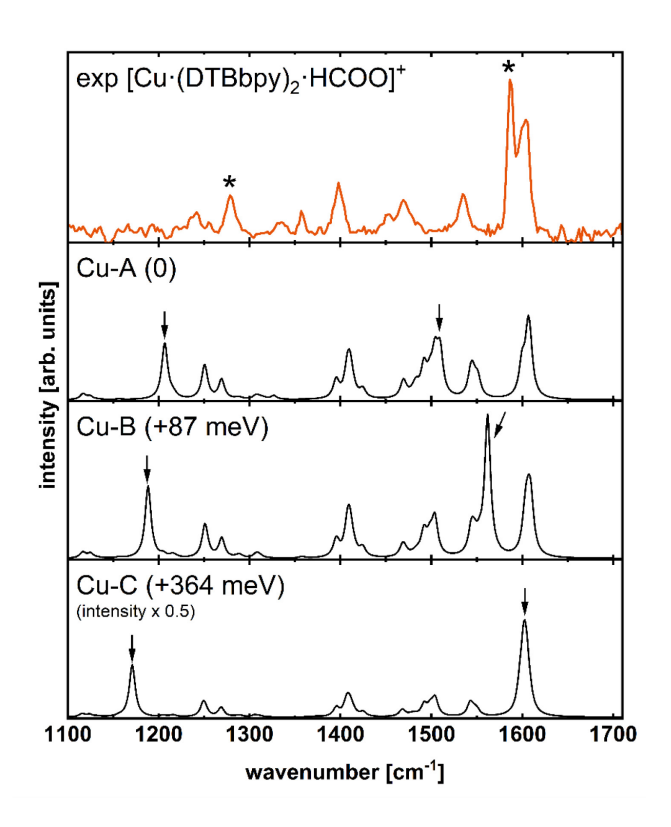


**Figure 7.** Comparison of the experimental spectra of  $[Cu \cdot (DTBbpy)_2 \cdot HCOO]^+$  (top trace, orange) with calculated spectra for the isomers of  $[Cu \cdot (DTBbpy)_2 \cdot HCOO]^+$  (bottom traces, black, isomer labels and relative energies given as in Table 3). The signatures of the formate OCO stretching vibrations in the experimental spectrum are marked with asterisks, while their positions in the calculated spectra are marked with arrows, with  $v_s$  being the lower frequency feature.

Table 3. Calculated energies and spin states of different isomers of  $[Cu \cdot (DTBbpy)_2 \cdot HCOO]^+$  complexes.

Complex	Relative Energy [meV]	Cu-O [pm]
Isomer Cu-A	0	201, 283
Isomer Cu-B	87	196, 334
Isomer Cu-C	364	194, 415

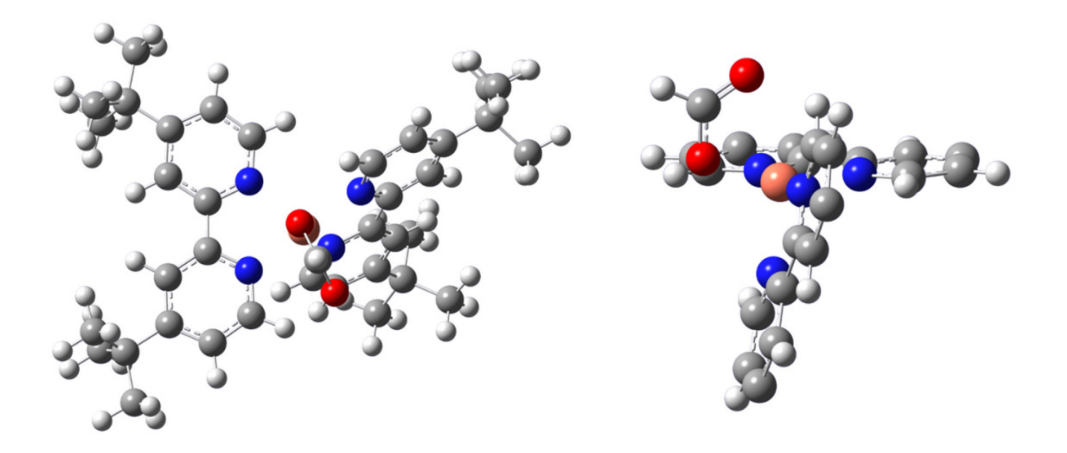


**Figure 8.** Lowest energy structure of  $[Cu \cdot (DTBbpy)_2 \cdot HCOO]^+$  (isomer Cu-A). **Left:** Structure viewed along the CH bond axis of the formate ligand to highlight the orientation of the formate relative to the metal atom. **Right:** Structure viewed from the side to highlight formate orientation relative to DTBBpy ligands, whose methyl groups are omitted for clarity. Color scheme: H = white, C = gray, N = dark blue, Cu = orange, O = red.

Formal discussion of electron configurations is typically based on integer charges, but the fractional charges produced by natural population analysis still lend themselves to a qualitative discussion. All metal atoms have charges between +0.87 e and +1.1 e, the formate ligands have charges between -0.60 e and -0.64 e, and the spin density is mostly localized on the metal atoms. This calculated charge distribution indicates in each case that there is significant charge transfer between the metal center, formate adduct, and organic ligands, and shows that the DTBbpy ligands act as charge reservoirs in each complex. While no population analysis should be considered exact, we note that the calculations predict significantly less than +2 e charge on each metal center despite that being their formal oxidation state. In combination with the large amount of charge accommodated by the DTBbpy ligands, this highlights how the ligand framework plays a role in modifying the redox properties of the complex by absorbing and releasing charge throughout different coordination regimes.

Table 4. Calculated charge distributions for each [M·(DTBbpy)2·HCOO]<sup>+</sup> complex from natural population analysis.

Complex	Metal	DTBbpy ligands	Formate
$[\text{Co}\cdot(\text{bpy-tBu})2]^{2+}$	0.877	1.123	-
$[\text{Co}\cdot(\text{bpy-tBu})_2\cdot\text{HCOO}]^+$	1.034	0.602	-0.636
(Isomer Co-QA)	1.034		
$[Ni \cdot (bpy-tBu)_2 \cdot HCOO]^+$	0.938	0.670	-0.608
(Isomer Ni-TA)	0.938		
$[Cu \cdot (bpy-tBu)_2 \cdot HCOO]^+$	0.986	0.650	-0.636
(Isomer Cu-A)	0.700	0.030	

The differences between the calculated charges, indicating a +1 oxidation state, and the spin density, which is more consistent with a +2 oxidation state, present a challenge for the interpretation of the interplay of electronic and geometric structural properties of the complexes. Multiple factors play into the structures of transition metal complexes with low symmetry, from simple electrostatic considerations to ligand field and symmetry arguments. For M = Cu, the Cu-N distance opposite to the O atom farthest from the metal is the longest among the Cu-N distances, at 222 pm, compared to 202 pm, 203 pm, and 209 pm. This suggests to view the structure of the complex as close to a Jahn-Teller distorted octahedral complex, with the long Cu-O and Cu-N distances indicating the axial ligands (see Figure 9). This interpretation is consistent with a  $d^9$  occupancy of the d-block in a Cu(II) complex, which is known to adopt extremely elongated octahedral structures due to degeneracy in the  $e_g$  orbital. Following this line of reasoning, the spin density, rather than the calculated total charge on the Cu atom, would dominate the primary structural characteristics of the coordination environment.

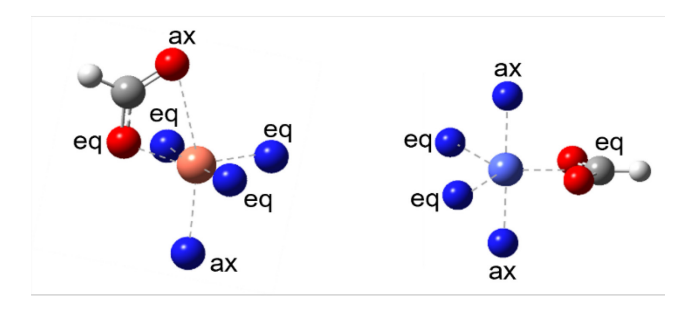


**Figure 9.** Approximation of the coordination environment for M = Cu as a Jahn-Teller distorted octahedral  $ML_6$  complex (left), and for M = Co and Ni as a trigonal bipyramidal  $ML_5$  complex (right). The axial and equatorial ligands are labeled as "ax" and "eq", respectively. Color scheme: H = white, C = gray, N = dark blue, Cu = orange, O = red, Co = light blue.

The structures for M = Co and Ni are less straightforward to interpret since they deviate significantly from an octahedral environment around the metal center (Figure 9). If considering the formate O atoms as individual ligands, the structure could be described as distorted trigonal antiprismatic with each triangular face constructed of one O atom and both N atoms of a DTBbpy ligand. The M = Co and Ni complexes may also be considered as trigonal bipyramidal ML<sub>5</sub> structures, where the formate would take the role of a single ligand despite its bidentate interaction with the metal. These two interpretations do not present obvious distinctions that would allow unique classification of the observed complex geometries. We hypothesize that the determining factor distinguishing the structural motifs for M= Cu vs. M = Co and Ni is the presence of some significant electronic degeneracy in the Cu complex that is not present in the Co and Ni compounds, resulting in distinct binding geometries. We therefore assume that simple electrostatic interactions provide the dominant contribution to the latter, while ligand field interactions are more decisive for the former.

#### **Conclusions**

We present vibrational spectra of bipyridine-based M-4N complexes with a formate adduct of the form [M·(DTBbpy)2·HCOO]<sup>+</sup>, where Co, Ni, or Cu were coordinated as the metal center. Through comparison with DFT calculations, we found that the modes associated with the DTBbpy ligands do not shift appreciably upon exchange of the metal center, but the OCO symmetric and antisymmetric stretching modes do respond to a change in metal identity. The calculated structures show a distorted octahedral coordination environment of the metal, and the complexes have approximately  $C_2$  symmetry for Co and Ni, while the Cu complex is non-symmetric. The formate ligand binds symmetrically to Co and Ni centers, and asymmetrically to Cu. The Co and Ni complexes are in their high-spin states, and the calculations indicate significant charge transfer throughout the complexes, with the DTBbpy ligands acting as charge reservoirs.

#### ASSOCIATED CONTENT

Supporting Information: Calculated structures of  $[Co\cdot(DTBbpy)_2]^{2+}$  and  $[M\cdot(DTBbpy)_2\cdot HCOO]^+$  (M = Co, Ni, Cu); calculated energies of  $[Co\cdot(DTBbpy)_2]^{2+}$  and of different isomers of  $[M\cdot(DTBbpy)_2\cdot HCOO]^+$  (M = Co, Ni, Cu) using UB3LYP/6-31G and  $\omega$ B97XD/6-31G; experimental and calculated formate OCO stretching frequencies, and calculated M-O distances in  $[M\cdot(DTBbpy)_2\cdot HCOO]^+$  complexes (M = Co, Ni, Cu); experimental spectra of  $[M\cdot(DTBbpy)_2\cdot HCOO]^+$  with calculated spectra for their isomers. The following files are available free of charge:

#### **AUTHOR INFORMATION**

# **Corresponding Author**

\*J. Mathias Weber – JILA and Department of Chemistry, University of Colorado, Boulder,

Colorado 80309-0440, United States; orcid.org/0000-0002-5493-5886; Phone: +1-303-492-7841;

Email: weberjm@jila.colorado.edu

#### Authors

Madison M. Foreman – JILA and Department of Chemistry, University of Colorado, Boulder, Colorado 80309-0440, United States

Rebecca J. Hirsch – JILA and Department of Chemistry, University of Colorado, Boulder, Colorado 80309-0440, United States

#### **Notes**

‡ Based on: Madison M. Foreman, Study on Metal-Ligand Interactions: Infrared Ion Spectroscopy of Coordination Compounds, PhD Thesis (2023) University of Colorado Boulder.

The authors declare no competing financial interests.

#### ACKNOWLEDGMENT

J.M.W. gratefully acknowledges support from the U. S. National Science Foundation under awards no. CHE-1764191 and CHE-2154271. This work utilized resources from the University of Colorado Boulder Research Computing Group, which is supported by the National Science Foundation (awards ACI-1532235 and ACI-1532236), the University of Colorado Boulder, and Colorado State University.

#### REFERENCES

- (1) Savéant, J.-M. Molecular Catalysis of Electrochemical Reactions. Mechanistic Aspects. *Chem. Rev.* **2008**, *108*, 2348–2378.
- (2) Sampson, M. D.; Froehlich, J. D.; Smieja, J. M.; Benson, E. E.; Sharp, I. D.; Kubiak, C. P. Direct Observation of the Reduction of Carbon Dioxide by Rhenium Bipyridine Catalysts. *Energy Environ. Sci.* **2013**, *6*, 3748.
- (3) Benson, E. E.; Kubiak, C. P.; Sathrum, A. J.; Smieja, J. M. Electrocatalytic and Homogeneous Approaches to Conversion of CO<sub>2</sub> to Liquid Fuels. *Chem. Soc. Rev.* **2009**, *38*, 89–99.
- (4) Costentin, C.; Robert, M.; Savéant, J.-M. Catalysis of the Electrochemical Reduction of Carbon Dioxide. *Chem. Soc. Rev.* **2013**, *42*, 2423–2436.
- (5) Smieja, J. M.; Kubiak, C. P. Re(Bipy-TBu)(CO)<sub>3</sub>Cl-Improved Catalytic Activity for Reduction of Carbon Dioxide: IR-Spectroelectrochemical and Mechanistic Studies. *Inorg. Chem.* **2010**, *49*, 9283–9289.
- (6) Costentin, C.; Drouet, S.; Robert, M.; Savéant, J.-M. A Local Proton Source Enhances CO<sub>2</sub> Electroreduction to CO by a Molecular Fe Catalyst. *Science* **2012**, *338*, 90–94.
- (7) Cosnier, S.; Deronzier, A.; Moutet, J.-C. Electrocatalytic Reduction of CO<sub>2</sub> on Electrodes Modified by Fac-Re(2,2'-Bipyridine)(CO)<sub>3</sub>Cl Complexes Bonded to Polypyrrole Films. *J. Molec. Catal.* **1988**, *45*, 381–391.
- (8) Rizzo, T. R.; Stearns, J. A.; Boyarkin, O. V. Spectroscopic Studies of Cold, Gas-Phase Biomolecular Ions. *Int. Rev. Phys. Chem.* **2009**, *28*, 481–515.

- (9) Yang, N.; Huchmala, R. M.; McCoy, A. B.; Johnson, M. A. Character of the OH Bend–Stretch Combination Band in the Vibrational Spectra of the "Magic" Number H<sub>3</sub>O<sup>+</sup>(H<sub>2</sub>O)<sub>20</sub> and D<sub>3</sub>O<sup>+</sup>(D<sub>2</sub>O)<sub>20</sub> Cluster Ions. *J. Phys. Chem. Lett.* **2022**, *13*, 8116–8121.
- (10) Kreinbihl, J. J.; Frederiks, N. C.; Johnson, C. J. Hydration Motifs of Ammonium Bisulfate Clusters Show Complex Temperature Dependence. *J. Chem. Phys.* **2021**, *154*, 014304.
- (11) Sherman, S. L.; Fischer, K. C.; Garand, E. Conformational Changes Induced by Methyl Side-Chains in Protonated Tripeptides Containing Glycine and Alanine Residues. *J. Phys. Chem. A* 2022, *126*, 4036–4045.
- (12) Jin, J.; Wulf, T.; Jorewitz, M.; Heine, T.; Asmis, K. R. Vibrational Spectroscopy of Cu<sup>+</sup>(H<sub>2</sub>)<sub>4</sub>: About Anharmonicity and Fluxionality. *Phys. Chem. Chem. Phys.* **2023**, *25*, 5262–5270.
- (13) Heller, J.; Cunningham, E. M.; van der Linde, C.; Ončák, M.; Beyer, M. K. Infrared Multiple Photon Dissociation Spectroscopy Confirms Reversible Water Activation in Mn<sup>+</sup>(H<sub>2</sub>O)<sub>n</sub>, n ≤ 8. J. Phys. Chem. Lett. 2022, 13, 3269–3275.
- (14) Xu, S.; Smith, J. E. T.; Weber, J. M. Ligand Influence on the Electronic Spectra of Dicationic Ruthenium-Bipyridine-Terpyridine Complexes. *J. Phys. Chem. A* **2016**, *120*, 2350–2356.
- Zagorec-Marks, W.; Dodson, L. G.; Weis, P.; Schneider, E. K.; Kappes, M. M.; Weber, J.
   M. Intrinsic Structure and Electronic Spectrum of Deprotonated Biliverdin: Cryogenic Ion
   Spectroscopy and Ion Mobility. J. Am. Chem. Soc. 2021, 143, 17778–17785.

- (16) Surendran, A. K.; Tripodi, G. L.; Pluhařová, E.; Pereverzev, A. Y.; Bruekers, J. P. J.; Elemans, J. A. A. W.; Meijer, E. J.; Roithová, J. Host-guest Tuning of the CO<sub>2</sub> Reduction Activity of an Iron Porphyrin Cage. *Nat. Sci.* **2023**, *3*, e20220019.
- (17) Chen, L.; Ma, Z.; Fournier, J. A. Origins of the Diffuse Shared Proton Vibrational Signatures in Proton-Coupled Electron Transfer Model Dyad Complexes. *J. Chem. Phys.* **2022**, *157*, 154308.
- (18) Dahlmann, F.; Dinu, D.; Jusko, P.; Lochmann, C.; Gstir, T.; Marimuthu, A.; Liedl, K.; Brünken, S.; Wester, R. Vibrational Predissociation Spectra of C<sub>2</sub>N<sup>-</sup> and C<sub>3</sub>N<sup>-</sup>: Bending and Stretching Vibrations. *ChemPhysChem* **2023**, e202300262.
- (19) Dopfer, O.; Nizkorodov, S. A.; Meuwly, M.; Bieske, E. J.; Maier, J. P. Microsolvation of the Ammonium Ion in Argon: Infrared Spectra of NH<sub>4</sub><sup>+</sup>–Ar<sub>n</sub> Complexes (n = 1–7). *Int. J. Mass Spectrom. Ion Proc.* **1997**, *167–168*, 637–647.
- (20) Tanabe, S.; Ebata, T.; Fujii, M.; Mikami, N. OH Stretching Vibrations of Phenol–(H<sub>2</sub>O)<sub>n</sub> (N=1–3) Complexes Observed by IR-UV Double-Resonance Spectroscopy. *Chem. Phys. Lett.* **1993**, *215*, 347–352.
- (21) Gorbachev, V.; Tsybizova, A.; Miloglyadova, L.; Chen, P. Increasing Complexity in a Conformer Space Step-by-Step: Weighing London Dispersion against Cation-π Interactions. J. Am. Chem. Soc. 2022, 144, 9007–9022.
- (22) Lin, S.; Diercks, C. S.; Zhang, Y.-B.; Kornienko, N.; Nichols, E. M.; Zhao, Y.; Paris, A. R.; Kim, D.; Yang, P.; Yaghi, O. M.; et al. Covalent Organic Frameworks Comprising Cobalt Porphyrins for Catalytic CO<sub>2</sub> Reduction in Water. *Science* 2015, 349, 1208–1213.

- (23) Beley, Marc.; Collin, J. Paul.; Ruppert, Romain.; Sauvage, J. Pierre. Electrocatalytic Reduction of Carbon Dioxide by Nickel Cyclam<sup>2+</sup> in Water: Study of the Factors Affecting the Efficiency and the Selectivity of the Process. *J. Am. Chem. Soc.* **1986**, *108*, 7461–7467.
- (24) Ogata, T.; Yanagida, S.; Brunschwig, B. S.; Fujita, E. Mechanistic and Kinetic Studies of Cobalt Macrocycles in a Photochemical CO<sub>2</sub> Reduction System: Evidence of Co-CO<sub>2</sub> Adducts as Intermediates. *J. Am. Chem. Soc.* **1995**, *117*, 6708–6716.
- (25) Hawecker, J.; Lehn, J.-M.; Ziessel, R. Electrocatalytic Reduction of Carbon Dioxide Mediated by Re(Bipy)(CO)<sub>3</sub>Cl (Bipy = 2,2'-Bipyridine). *J. Chem. Soc., Chem. Commun.* **1984**, 328–330.
- (26) Keith, J. A.; Grice, K. A.; Kubiak, C. P.; Carter, E. A. Elucidation of the Selectivity of Proton-Dependent Electrocatalytic CO<sub>2</sub> Reduction by *Fac*-Re(Bpy)(CO)<sub>3</sub>Cl. *J. Am. Chem. Soc.* **2013**, *135*, 15823–15829.
- (27) Tanaka, K.; Ooyama, D. Multi-Electron Reduction of CO<sub>2</sub> via Ru–CO<sub>2</sub>, –C(O)OH, –CO, –CHO, and –CH<sub>2</sub>OH Species. *Coord. Chem. Rev.* **2002**, *226*, 211–218.
- (28) Manbeck, G. F.; Fujita, E. A Review of Iron and Cobalt Porphyrins, Phthalocyanines and Related Complexes for Electrochemical and Photochemical Reduction of Carbon Dioxide. *J. Porphyr. Phthalocyanines* **2015**, *19*, 45–64.
- (29) Takeda, H.; Koizumi, H.; Okamoto, K.; Ishitani, O. Photocatalytic CO<sub>2</sub> Reduction Using a Mn Complex as a Catalyst. *Chem. Commun.* **2014**, *50*, 1491–1493.

- (30) Beley, M.; Collin, J.-P.; Ruppert, R.; Sauvage, J.-P. Nickel(II)-Cyclam: An Extremely Selective Electrocatalyst for Reduction of CO<sub>2</sub> in Water. *J. Chem. Soc., Chem. Commun.* **1984**, 1315-1316.
- (31) Weng, Z.; Jiang, J.; Wu, Y.; Wu, Z.; Guo, X.; Materna, K. L.; Liu, W.; Batista, V. S.; Brudvig, G. W.; Wang, H. Electrochemical CO<sub>2</sub> Reduction to Hydrocarbons on a Heterogeneous Molecular Cu Catalyst in Aqueous Solution. J. Am. Chem. Soc. 2016, 138, 8076–8079.
- (32) Foreman, M. M.; Hirsch, R. J.; Weber, J. M. Effects of Formate Binding to a Bipyridine-Based Cobalt-4N Complex. *J. Phys. Chem. A* **2021**, *125*, 7297–7302.
- (33) Xu, S.; Gozem, S.; Krylov, A.I.; Cristopher, C. R.; Weber, J. M. Ligand influence on the electronic spectra of monocationic copper–bipyridine complexes. *Phys. Chem. Chem. Phys.* **2015**, *17* (47), 31938-31946.
- (34) Becke, A. D. Density-functional Thermochemistry. III. The Role of Exact Exchange. *J. Chem. Phys.* **1993**, *98*, 5648–5652.
- (35) Hay, P. J.; Wadt, W. R. *Ab Initio* Effective Core Potentials for Molecular Calculations. Potentials for K to Au Including the Outermost Core Orbitals. *J. Chem. Phys.* **1985**, *82*, 299–310.
- (36) Chai, J.-D.; Head-Gordon, M. Long-Range Corrected Hybrid Density Functionals with Damped Atom-Atom Dispersion Corrections. *Phys. Chem. Chem. Phys.* **2008**, *10* (44), 6615.
- (37) Dunning, T. H. Gaussian Basis Sets for Use in Correlated Molecular Calculations. I. The Atoms Boron through Neon and Hydrogen. *J. Chem. Phys.* **1989**, *90*, 1007–1023.

- (38) Weigend, F. Accurate Coulomb-Fitting Basis Sets for H to Rn. *Phys. Chem. Chem. Phys.* **2006**, *8*, 1057.
- (39) Frisch, M. J.; Trucks, G. W.; Schlegel, H. B.; Scuseria, G. E.; Robb, M. A.; Cheeseman, J.
   R.; Scalmani, G.; Barone, V.; Petersson, G. A.; Nakatsuji, H., et al. *Gaussian 16 Rev. C.01*,
   Wallingford, CT, 2016.
- (40) Gerardi, H. K.; DeBlase, A. F.; Su, X.; Jordan, K. D.; McCoy, A. B.; Johnson, M. A. Unraveling the Anomalous Solvatochromic Response of the Formate Ion Vibrational Spectrum: An Infrared, Ar-Tagging Study of the HCO<sub>2</sub>, DCO<sub>2</sub>, and HCO<sub>2</sub>·H<sub>2</sub>O Ions. *J. Phys. Chem. Lett.* **2011**, *2*, 2437–2441.
- (41) Dodson, L. G.; Thompson, M. C.; Weber, J. M. Characterization of Intermediate Oxidation States in CO<sub>2</sub> Activation. *Annu. Rev. Phys. Chem.* **2018**, *69*, 231–252.
- (42) Cotton, F. A.; Wilkinson, G. *Advanced Inorganic Chemistry*, 3rd ed.; John Wiley & Sons, 1972; pp 528-1077.

# **TOC GRAPHICS**

